REVISTA DE
ARQUITETURA IMED

Geospatial analysis in assessing environmental sustainability levels

Análise geoespacial na avaliação dos níveis de sustentabilidade ambiental

Cezar Isadora Caino(1); Julia Scopel(2); Julia Almeida(3); Brian Bodah(4); M. Santosh(5); Alcindo Neckel(6)

1 Doutoranda Ciências e Engenharia de Materiais – UFSC.
E-mail: isadoracain@gmail.com | ORCID: https://orcid.org/0000-0001-7194-9414
2 Graduanda em Arquitetura e Urbanismo da Escola Politécnica da ATITUS Educação.
E-mail: juliascopel10@gmail.com | ORCID: https://orcid.org/0009-0000-1356-0531
3 Graduanda em Arquitetura e Urbanismo da Escola Politécnica da ATITUS Educação.
E-mail: julia.allm659@gmail.com | ORCID: https://orcid.org/0009-0002-7158-6961
4 Doutor Biological Systems Engineering from Washington State University.
E-mail: brian.bodah.777@gmail.com | ORCID: https://orcid.org/0009-0004-6920-1107
5 Professor PhD in Ciencie - China University of Geosciences.
E-mail: santosh@cugb.edu.cn | ORCID: https://orcid.org/0000-0002-1073-8477
6 Professor PhD in Geography and Environmental Sciences – ATITUS Educação.
E-mail: alcindo.neckel@atitus.edu.br | ORCID: https://orcid.org/0000-0001-5435-3096

Revista de Arquitetura IMED, Passo Fundo, vol. 15, n. 1, p. 90-107, janeiro-junho, 2026 - ISSN 2318-1109

DOI: https://doi.org/10.18256/2318-1109.2026.v15i1.5382

Sistema de Avaliação: *Double Blind Review*

Abstract

Geospatial analyzes are becoming fundamentally important on a global scale for the sake of sustainability. The overall objective of this research is to analyze geospatial data, using images from Landsat 2, 5, 7, and 8 satellites from 1975 to 2020, based on changes in land use, and from Sentinel-3B OLCI (Ocean Land Color Instrument) from 2019 to 2021, focusing on the evaluation of water resources based on water turbidity levels (TSM_NN), suspended particle density (ADG_443_NN), and chlorophyll-a presence (CHL_NN), aiming to temporally monitor the effectiveness of current legislation on sustainability standards in a watershed region dedicated to agricultural production, located in southern Brazil. Satellite images from Sentinel-3B OLCI between 2019 and 2021 showed that the waters of the Capinguí Dam have high concentrations of ADG_443_NN (3,830 m-1), CHL_NN (20,290 (mg m-3)) and TSM_NN (100 (gm -3)), capable of endangering the health of the population and the hydrographic preservation.

Keywords: landscape metrics; land use change; SDG; food securit; Remote sensing.

Resumo

As análises geoespaciais tornam-se de fundamental importância em escala global, em prol da sustentabilidade. O objetivo geral desta pesquisa é analisar de forma geoespacial, por meio de imagens dos satélites Landsat 2, 5, 7, 8 no período de 1975 a 2020 com base nas mudanças no uso do solo, e do Sentinel-3B OLCI (Ocean Land Color Instrument), no período de 2019 a 2021 voltados a avaliação dos recursos hídricos, com base nos níveis de turbidez da água (TSM_NN), potencial de poluição suspensa (ADG_443_NN) e presença de clorofila-a (CHL_NN), visando acompanhar de forma temporal a efetividade da legislação vigente, sobre os padrões de sustentabilidade, numa região de bacia hidrográfica voltada à produção agrícola, localizada ao sul do Brasil. As imagens do satélite Sentinel-3B OLCI no período de 2019 e 2021, demonstraram que as águas da Barragem do Capinguí possuem concentração elevada de ADG_443_NN (3.830 m-***1***), CHL_NN (20,290 (mg m-***3***)) e TSM_NN (100 (gm -3)), capazes de colocar em risco a saúde da população e a preservação hidrográfica.

Palavras-chave: Paisagem métricas; Mudança no uso da terra; ODS; Segurança alimentar; Sensoriamento remoto.

1 Introduction

Changes in agricultural land use in river basins globally have proven unsustainable due to the continuous environmental degradation they cause, thus increasingly requiring the formulation of public policies aimed at implementing recovery projects capable of mitigating potential harmful effects on the environment (Chowdhury et al., 2022). In an attempt to understand the environmental degradation processes involved in changes in land use and occupation, it is of fundamental importance to monitor and control the factors related to increased agricultural production, aiming at the sustainability of the process and food security (Viana et al., 2022). This monitoring and control also contribute to the Sustainable Development

Goals (SDGs) through the analysis of each territory, considering that each region has distinct peculiarities and inequalities, increasing the complexity of studies and mitigation and adaptation strategies (Acuti, Bellucci, Manetti, 2020).

The SDGs include 17 goals, 169 targets, and 231 indicators, where 193 UN member countries have committed to practical actions for the success of these goals aimed at the sustainability of the planet (Acuti, Bellucci, Manetti, 2020). In this context, they address crucial themes for humanity and the environment, such as food production, related to food security, sustainable agriculture, and responsible production and consumption (Viana et al., 2022). Due to the use of agricultural land in watershed areas, and the need to increase food production on a global scale, the need for geospatial studies related to environmental preservation is increasingly justified (Parven et al., 2022).

It is worth remembering that geospatial studies are tools that assist in analysis and decision-making to promote local and global development (Goodchild, 2007). In addition, climate change and land conservation issues are part of the 17 Sustainable Development Goals of the United Nations (UN), which require actions and initiatives to combat climate fluctuations, as well as protect life on Earth (United Nations, 2015). These factors related to sustainability lead to positive issues regarding agricultural cultivation areas, aimed at meeting food demands sustainably, achieving local and global intensification (FAO, 2017). This justifies the importance of conducting this study for society, considering sustainability standards in relation to a hydrographic region of agricultural cultivation in southern Brazil (Rockström et al., 2009).

Studies involving images from the Landsat 2, 5, 7, and 8 satellites, and the Sentinel-3B OLCI, aimed at accumulating terrestrial information by wavelength, have allowed for detailed, highly reliable analyses of land use and water resources globally, from January 22, 1975 (the year Landsat 2 was launched) to the present day with the use of the Landsat-8 satellite, launched on February 11, 2013, and the Sentinel-3B OLCI, launched into space orbit on February 16, 2016 (Wulder et al., 2019). It is worth remembering that the images from the Sentinel-3B OLCI satellite allow for precise analysis of water quality in river basins, related to the environmental impact caused by agricultural cultivation at micro and macro scales, related to water turbidity levels (TSM_NN), suspended pollution potential (ADG_443_NN), and the presence of chlorophyll-a (CHL_NN) (Toming et al., 2017).

The use of images from Landsat 2, 5, 7, 8 and Sentinel-3B OLCI satellites can provide parameters that allow the identification of land uses, highlighting agricultural areas, water resources, forests and urbanized areas, thus highlighting the changes that have occurred in land use and, through studies, it is possible to understand the variations that have occurred in certain locations within a period of time (Wulder et al., 2019; Roy et al., 2014).

The overall objective of this study is to analyze, geospatially, using Landsat 2, 5, 7, and 8 satellite images from 1975 to 2020, based on changes in land use, and Sentinel-3B OLCI images from 2019 to 2021, focusing on the assessment of water resources based on TSM_NN, ADG_443_NN, and CHL_NN levels, aiming to monitor the effectiveness of current legislation over time regarding sustainability standards in a hydrographic basin region focused on agricultural production, located in southern Brazil (Donlon et al., 2012; Toming et al., 2017). This study becomes extremely important by relating agricultural evolution patterns, characteristic of food security reinforced by the UN, with land use and water resource quality from a geospatial perspective, based on the effectiveness of relevant legislation in Brazil (Viana et al., 2022).

2 Materials and Methods

2.1 Study Area

The object of study consists of agricultural areas in the Passo Fundo River Basin, surrounding the Capinguí Dam regulating reservoir, which is located in the rural areas of the cities of Passo Fundo, Marau, and Mato Castelhano, in the state of Rio Grande do Sul, in southern Brazil (Figure 1). The city of Passo Fundo has an estimated population in 2019 of 203,275 inhabitants, with a population density of 235.9 inhabitants/km^2, considering (IBGE, 2019).

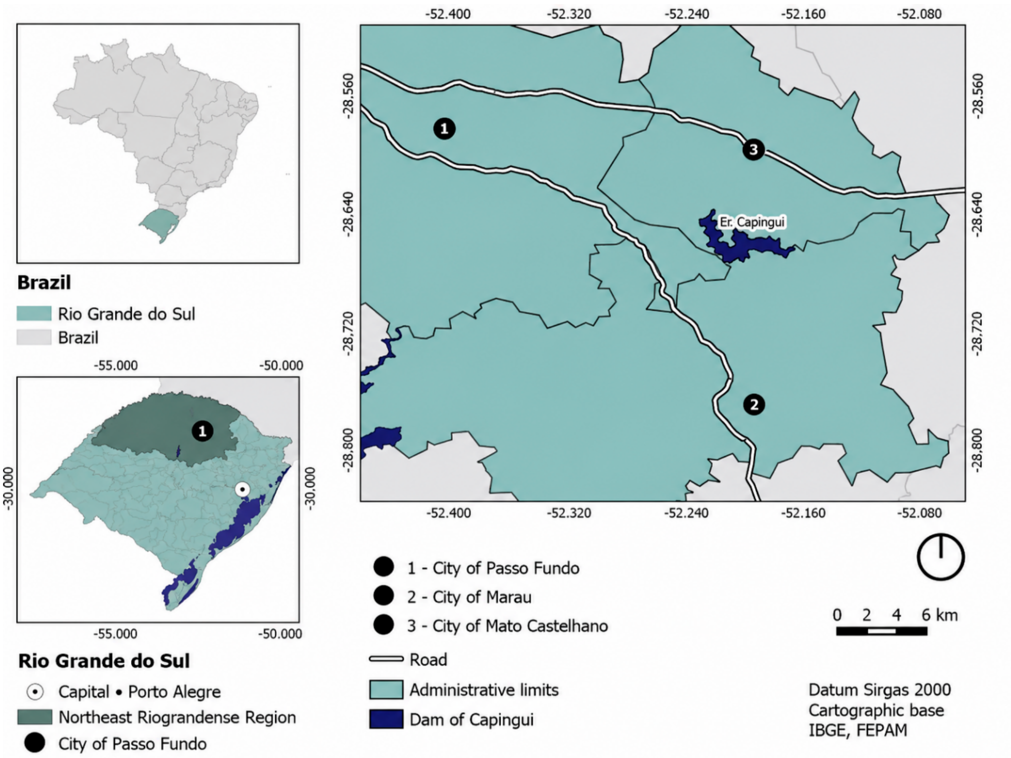

Figure 1: Location of the study areas (Passo Fundo, Marau and Mato Castelhano), in relation to the state of Rio Grande do Sul/Brazil. **Source:** Adapted from the IBGE geographic database.

The Capinguí Dam was built by CEEE (Companhia Estadual de Energia Elétrica) for the operation of the Capinguí Hydroelectric Power Plant from 1933 onwards, intended for the generation of electricity, but currently serves as a public water supply. It is worth highlighting that the agricultural production area studied corresponds to the rural areas of the cities of Passo Fundo, Marau and Mato Castelhano located around the Capinguí Dam, which in 1975 totaled an area of 111,283,200 m² (CEEE, 2020). Therefore, the total area of this study was equivalent to 111,283,200 m², as it is an area of intense monitoring by environmental agencies around this water resource, with effective compliance with Brazilian environmental legislation, due to the influence of the Capinguí Dam (Donlon et al., 2012; Toming et al., 2017).

2.2 Data Collection Instrument

Land use maps of the study area were created from Landsat satellite images (Table 1). The images were obtained from the United States Geological Survey (USGS) website and processed using QGIS - Geographic Information System software, version 2.18. Regarding the dates of the satellite images, the most similar temporalities were used. In addition, the images were selected for their low cloud cover, thus ensuring adequate visibility levels applied to the analysis área (Roy et al., 2014).

Table 1. Planning to obtain and process Landsat satellite images

Satellite	Sensor	Worldwide Reference System	Collection date	Bands/RGB
Landsat 2	MSS	Path 238; Row 079	March 10th, 1975	RGB674
Landsat-5	TM	Path 222; Row 080	March 1st, 1985	RGB543
Landsat-5	TM	Path 222; Row 080	March 2nd, 1992	RGB543
Landsat-7	ETM	Path 222; Row 080	March 5th, 2001	RGB432
Landsat-5	TM	Path 222; Row 080	March 9th, 2011	RGB543
Landsat-8	OLI	Path 222; Row 080	March 17th, 2020	RGB654

The construction of land use maps went through a series of procedures, as demonstrated by the following steps: The first step was the construction of map mosaics by visualizing false colors in the Red, Green, and Blue (RGB) system. For this, different bands were used, depending on the characteristics and specificity of the Landsat satellite (Roy et al., 2014; Wulder et al., 2019). For the land use classification step, classes were pre-determined: water resource, agricultural land, forest, and exposed soil (Karasiak, 2016; QGIS Development Team, 2020). Subsequently, supervised classification was performed using the Dzetsaka tool in the QGIS software, adopting the Gaussian model (autor, ano). This classification of satellite images generated two raster (tif) files, processed with the Sieve tool in the QGIS software. This tool aims to remove raster polygons smaller than a certain size limit (in pixels) and replace them with the pixel value of the largest neighboring polygon, in addition to eliminating fragments, joining the predominant morphological characteristics (QGIS Development Team, 2020).

Subsequently, the data collected from Landsat 2, 5, 7, and 8 satellite images were subjected to landscape metrics, which consist of using various statistics to analyze the landscape (Turner, Gardner, O'Neill, 2001). To obtain the landscape metrics, the Lecos (Landscape Ecology Statistics) tool in the QGIS software was used. According to Jung, it is possible to verify the statistics across the entire landscape, allowing the calculation of various metrics in raster layers provided by the satellite images. In this context, the landscape metric analysis of this study was structured in the following procedures: statistical analysis of landscape composition and statistical analysis of landscape configuration, where the following were measured: Land cover (LC); Landscape proportion (PLAND); Patch density (PD); Largest patch index (LPI); Largest patch area (GPA); and total core area (TCA). The following metrics were used: Number of Patches (NP); Patch density (PD); Average patch area (AREA_MN); Median patch area (AREA_MD); Total Edge (TE); Edge density (ED); Fractal Dimension Index (FRAC); Mean Shape Index (MSI); Percentage of Adjacencies Like (PLADJ); Landscape Division Index (DIVISION); Patch Cohesion Index (COHESION); Effective Mesh Size (EM); Division Index (SI) (McGarigal, Cushman, Ene, 2012).

2.3 Water Quality Analysis of the Capinguí Dam

The water quality study for the Capinguí Dam was carried out using images from the Sentinel-3B OLCI satellite, Water Full Resolution (WFR) provided by the European Space Agency (ESA), with a resolution of 300 meters, considering a maximum standard error of 0.83 μg/mg in the analysis, adding to this study a 6.25% error, since these are images already calibrated by the ESA (ESA, 2021; Donlon et al., 2012). To perform the retrospective analyses, it was necessary to select images with a low percentage of clouds (Table 2). It is noted that obtaining satellite images of the cities of Passo Fundo, Marau, and Mato Castelhano is difficult because the region has a humid subtropical climate (Cfa), with consistent rainfall and an average annual temperature of 22°C, resulting in constant evaporation (Alvares et al., 2013).

Table 2. Satellite image date Sentinel-3B OLCI – WFR

2019	**Period**	**Image date**
Summer	21/12 to 20/03	2019/02/28
Autumn	21/3 to 20/6	2019/06/07
Winter	21/6 to 20/9	2019/09/04
Spring	21/9 to 20/12	2019/12/11
2021	**Period**	**Image date**
Summer	21/12 to 20/03	2021/03/12
Autumn	21/3 to 20/6	2021/06/14
Winter	21/6 to 20/9	2021/08/31
Spring	21/9 to 20/12	2021/10/27

Image processing was performed using Geographic Information System (GIS) software, SNAP version 8.0.4. To verify water quality, three analyses were performed (TSM_NN, ADG_443_NN and CHL_NN). The 37 satellite collection points were positioned at the Capingui Dam (Donlon et al., 2012; ESA, 2021; Toming et al., 2017).

2.4 Statistical analysis between classes

The data collected from Landsat 2, 5, 7, 8 and Sentinel-3B OLCI satellite images were analyzed using Pearson correlation, aimed at verifying the relationship between the classes of data collected (Schober, Boer & Schwarte, 2018). The "r" values in this method range from 1 to -1, with values close to zero meaning null correlation, that is, there is no influence of one variable on the other. If it is close to the value 1, it means that the increase of one variable influences the increase of another variable. While, when approaching -1, it means that the increase of one variable influences the reduction of the other variable. Regarding the interpretation, a correlation of 0.00 to 0.19 is considered very weak; 0.20 to 0.39 are weak; 0.40 to 0.69 are moderate; 0.70 to 0.89 and 0.90 to 1 are very strong. The analysis was performed using JASP software, version 0.13.1.0 (Schober, Boer & Schwarte, 2018).

For K-means clustering, the datasets collected by satellite were combined and organized into a single database. K-means clustering generated the Silhouette index, which displays the average internal consistency of the cluster by assessing the similarity of the data collected in the satellite images (Xu & Tian, 2015; Arbelaitz et al., 2013).

3. Results and Discussion

3.1 Land use and occupation through analysis of Landsat 2, 5, 7 and 8 satellite images

The proposed time frame is from 1975 to 2020, using data collected from Landsat 2, 5, 7 and 8 satellite images, which were analyzed based on the following classes: water resources, agricultural land, forest and exposed soil (Roy et al., 2014). Figure 2 (a) shows that in 1975 the cross-section showed 57.3% land cover by forest, the agricultural area corresponded to 23.9% and the exposed soil was 17.5%. In Figure 2 (b), in 1985, the agricultural area represented 31.7%, while forest cover was 31.6% and exposed soil represented 28.8%. In Figure 2(c), in 1992 the agricultural area increased to 23.3%, forest cover to 28.1%, and exposed soil corresponded to 47.3% of the analyzed section. In Figure 2(d), in 2001 the agricultural area corresponded to 30.9%, the forest area totaled 22.5%, and exposed soil corresponded to 44.8%. Figure 2(e) showed that in 2011, agriculture totaled 37.5%, while the forest area corresponded to 21.1%, and the exposed soil surface was 33.2%. In Figure 2(f), for 2020, the agricultural area corresponds to 31.4%, the forest area corresponds to 28.6%, and the exposed soil surface is 38.6% (Wulder et al., 2019).

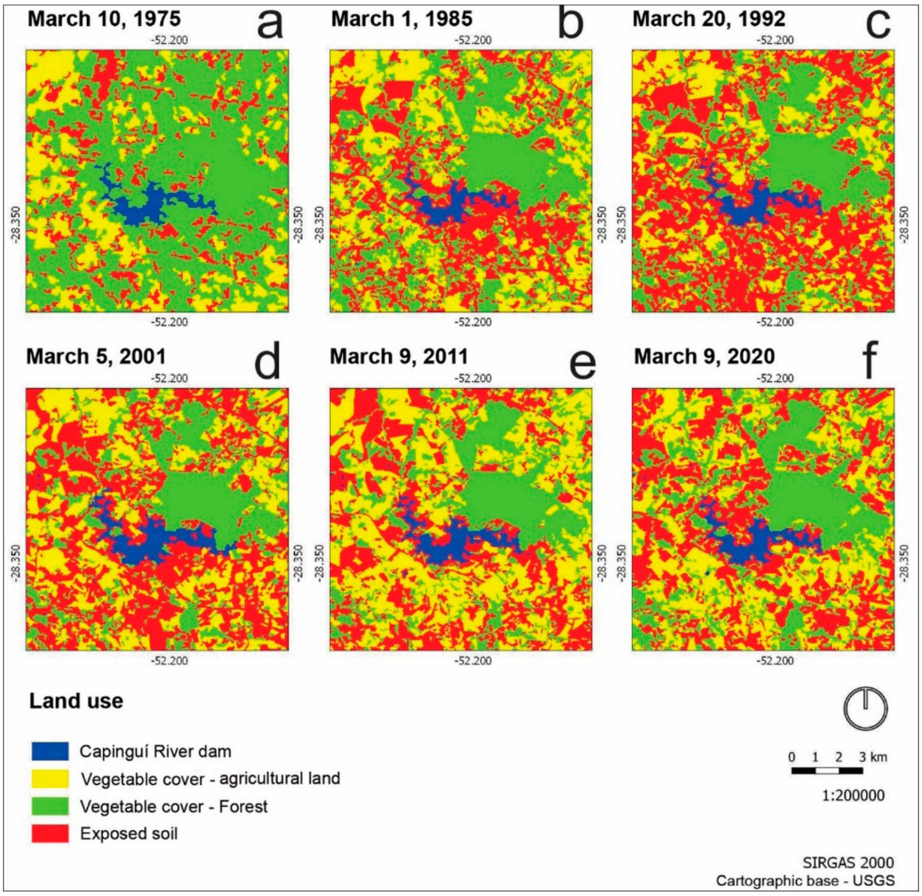

Figure 2: Images from Landsat 2, 5, 7, and 8 satellites over the study area: (a) 1975, (b) 1985, (c) 1992, (d) 2001, (e) 2011, and (f) 2020.

Through Figure 3, the histograms, structured in classes, allow for an understanding of the landscape transformation in the years 1975, 1992, 2001, and 2020. Interesting issues are observed, such as the significant difference in class proportions in 1975; the increase in arable areas in 1985; the gradual decline of forest cover and the predominance of exposed soil in the years 1992 and 2001, where the trend line demonstrates a stabilization of landscape transformation for the periods of 2001, 2011, and 2020 (Viana et al., 2022).

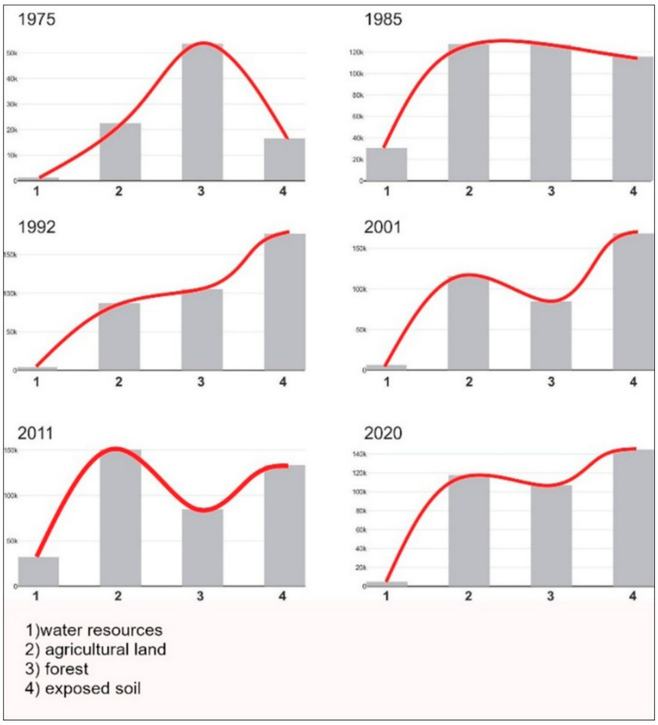

Figure 3: Land use in the area of interest: (a) 1975; (b) 1985; (c) 1992; (d) 2001; (e) 2011; and (f) 2020.

3.2 Analysis of landscape composition

The analysis of the landscape composition of the analyzed area was measured according to the following metrics: Area class (AC); Landscape Proportion (PLAND); Major Patch Index (LPI); Total Central Area (TCA). The cover (AC), in particular, an agropastoral area, had an agricultural area corresponding to 8,051.76 ha in 1975 and increased to 10,583.55 ha in 2020. The soil class had an exposed surface area of 5,886.72 ha in 1975 and changed to a surface area of 13,012.02 ha in 2020. The Forest class, in turn, had a surface area of 19,263.24 ha in 1975, and in 2020, an area corresponding to 9,631.98 ha (Figure 4(a)). This metric is an interesting tool for varying the proportions that do not show the result of different types of land use.

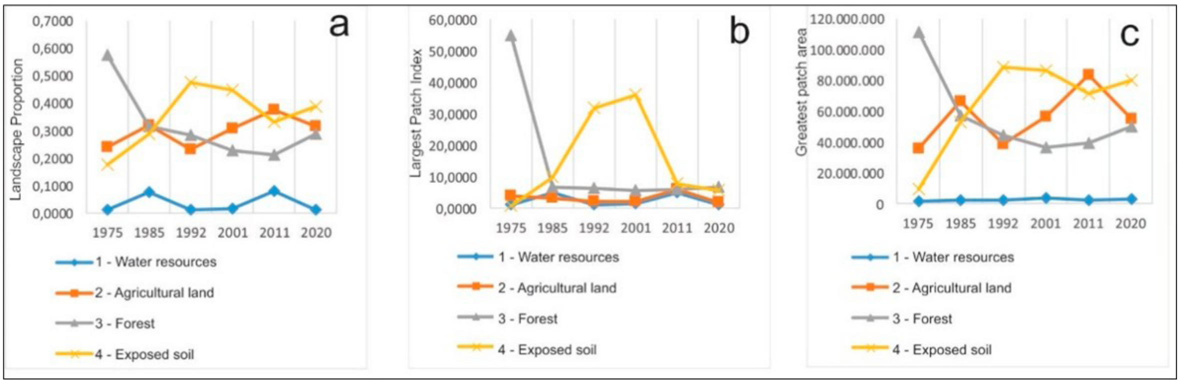

Figure 4: (a) Landscape Proportion (PLAND); (b) Largest Patch Index (LPI); (c) Greatest patch area (GPA); (d) Total Core Area (TCA).

Regarding the analysis of the percentage of the Largest Patch Index (LPI), it becomes represented with more significant interconnectivity between the patches of each class. In Figure 4 (b), it was found that the connection process between the agricultural plots has been decreasing since 1975, as the index corresponded to 3.7660, and in 2020 it totaled 1.9656. In the exposed soil class of the years 1992 and 2001, they present an LPI of 31.8094 and 36.0303, respectively, demonstrating that there was high continuity between the patches (McGarigal, Cushman, Ene, 2012).

Figure 4 (c) shows the TCA in 1975 corresponding to an area of 111,283,200 m², a reduction process that began until 2001 with an area of 36,325,313 m². Up to 2011, with an area of 39,323,700 m², the TCA analysis demonstrates that a process of consolidation of the forest class is underway in the analyzed area. In 2020, with an area of 49,850,100 m², there is an increase of 27.2% compared to 2001 (Turner, Gardner, O'Neill, 2001).

3.3 Statistical analysis of the landscape extracted from Landsat 2, 5, 7 and 8 satellite images

The statistical analysis regarding the configuration of the rural landscape of the studied area was structured in the following metrics: Number of Patches (NP); Patch Density (PD); Average Patch Area (AREA_MN); Median Patch Area (AREA_MD); Total Edge (TE); Fractal Dimension Index (FRAC); and Edge Density (ED). Thus, it is highlighted that the number of patches (NP) is a measure that characterizes a given class, these attributes contribute to the understanding of the landscape characteristics. According to Figure 5 (a), with regard to the forest class, it is possible to observe a process of homogenization and densification, as the number of patches decreased by 22.6% from 1992 to 2020 (McGarigal, Cushman, Ene, 2012).

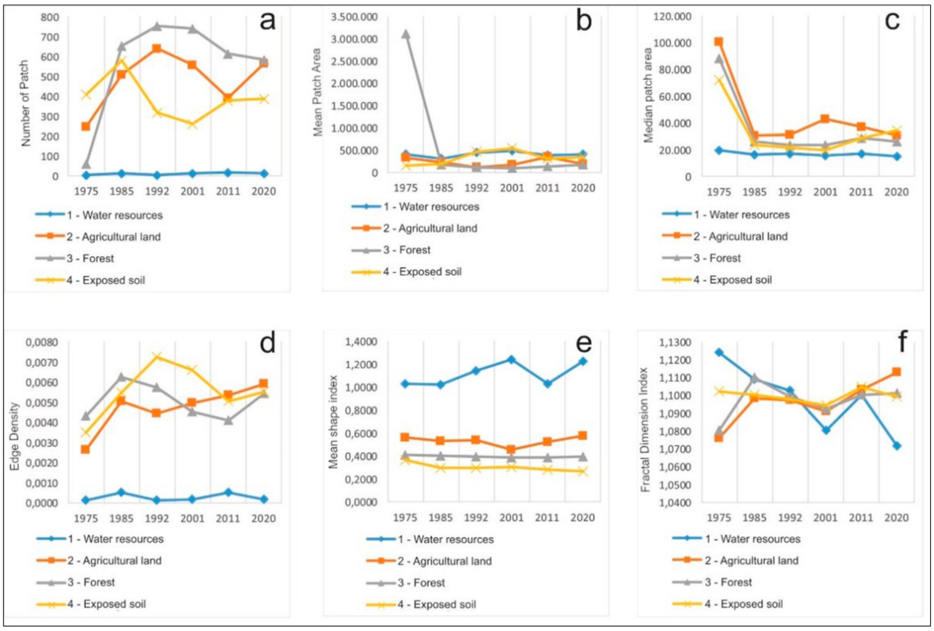

Figure 5: (a) Number of Patch (NP); (b) Mean Patch Area (AREA_MN); (c) Median patch area (AREA_MD); (d) Edge Density (ED); (e) Mean shape index (MSI); (f) Fractal Dimension Index (FRAC).

According to Figure 5 (b), the average size of the patches is smaller when compared to the classes intended for cultivation throughout the historical series, excluding the year 1975. Edge density (ED) is the edge length divided by the ground cover (LC). Observing Figure 5 (d), it was found that the increase in edge perimeter was more intense in the agricultural land class and the forest class showed a decrease in edge density (Turner, Gardner, O'Neill, 2001).

Regarding the analysis of the average shape index (MSI), it refers to the ratio between the perimeter of a patch and the perimeter of the simplest patch in the same class and measures the complexity of the shape. The MSI measurement, whose values are equal to 1, for the maximum degree of compactness, and if closer to zero, demonstrates how irregular the patch is (autor, ano). In Figure 5 (e), the values of the water resources class close to 1 validate this method, since the water resources are concentrated in the Capinguí Dam. The values for agricultural areas were 0.5603 in 1975 and 0.5795 in 2020, indicating a certain regularity in the shape of the patches. The values for the exposed soil class were 0.3675 in 1975 and 0.2624 in 2020, signifying the increasing regularity and continuity necessary for cultivation geared towards agribusiness (Li, Wu, 2004). The forest class has an MSI of 0.4071 in 1975 and 0.3968 in 2020, thus it can be said that despite the decrease in forest area, the patch shows low variation and contiguity.

The limits of this metric range from 1, for a relatively simple patch, to 2, for patches with more complex and convoluted shapes. Through Figure 5 (f), it can be observed that the classes of agricultural land, exposed soil and forest have FRAC from 1.07 to 1.11, with low variation, demonstrating the regularity of the patches over time.

3.4 Landscape fragmentation from Landsat 2, 5, 7 and 8 satellite images

Landscape fragmentation can be analyzed using some statistical metrics such as Percentage of Similar Adjacencies (PLADJ); Patch Cohesion Index (COHESION); effective mesh size (EM); and Division Index (SI). In this relationship, the degree of connectivity is measured by the Percentage of Similar Adjacencies (PLADJ), which calculates how many similar pixels are aggregated, with values close to zero signifying the level of disaggregation and values close to 1 representing greater aggregation. In Figure 6 (a), water resources are more aggregated, demonstrating the validity of the measurement, as the most significant patch is the Capinguí Dam (Uuemaa et al., 2013).

Another important metric is the Patch Cohesion Index (COHESION), which defines the ability of species to migrate between patches and also measures the physical connection of patches within a class, where patch cohesion increases as the patch type becomes more aggregated in its distribution and more connected. Through Figure 6 (b), it can be seen that the classes were homogeneous in terms of cohesion and connection, which becomes higher from 1985 onwards, with rates starting at 9.8 (Cushman, 2016).

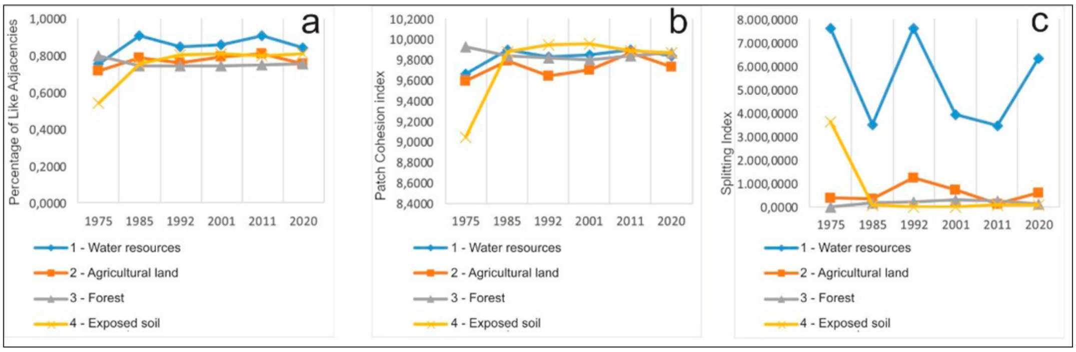

Figure 6: (a) Percentage of Like Adjacencies (PLADJ); (b) Patch Cohesion index (COHESION); (c) Splitting Index (SI).

In Figure 6 (d), it can be observed that the forest class was in the process of division and since 2011 this process has changed, as the SI has decreased. In relation to the agricultural land class, the division increased until 1992 and, after this period, the SI began to decrease, indicating a tendency for agglomeration between the patches, indicating greater homogeneity and consolidation of agricultural lands (Yiran et al., 2020).

3.5 Analysis of Sentinel-3B OLCI Satellite Images

In this stage, the compositions of the Sentinel-3B OLCI images were analyzed due to the importance of the Capinguí Dam for the study region. Thus, local data were considered, such as the average rainfall by season (Toming et al., 2017). For 2019, summer 160.3mm; autumn 158.8mm; winter 68.6 mm; spring 169.4 mm. For 2021, the rainfall regime presented the following situation: summer 138.4 mm; autumn 106.7

mm; Winter 99.16 mm; Spring 139.7 mm. Figure 7 shows the compositions of the Sentinel-3B OLCI images for ADG443_NN. In 2019 (Figure 7 (D)), the autumn season showed the highest concentration of suspended material on the water surface with a value of 3,830 m-1, followed by winter, with a value of 2,920 m-1 (Toming et al., 2017).

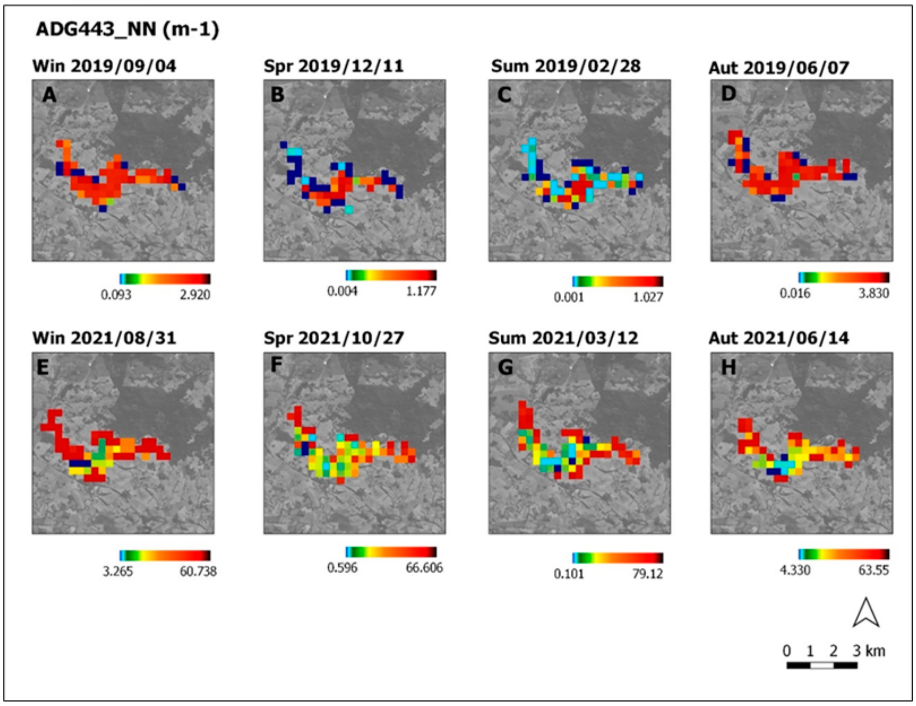

Figure 7: Composite Sentinel-3B OLCI images for dissolved material at the surface (ADG443_NN). (A) Winter 2019; (B) Spring 2019; (C) Summer 2019; (D) Autumn 2019; (E) Winter 2021; (F) Spring 2021; (G) Summer 2021; (H) Autumn 2021.

Figure 8 shows the composition of Sentinel-3B OLCI images focused on chlorophyll-a concentrations. In the analyzed period of 2019 (Figure 8 (D)), the autumn season presented the highest chlorophyll-a concentration with a value of 20,290 (mg (CHL_NN) m-3), followed by winter (Figure 8 (A)), with a value of 18,290 (mg (CHL_NN) m-3). Chlorophyll-a concentrations for the year 2021 decreased in all seasons, meaning lower chlorophyll concentration in the water and, consequently, less phytoplankton. The summer season (Figure 8(C and G)) shows the lowest chlorophyll values, which can be explained by the dry season characteristic of this period in the study region.

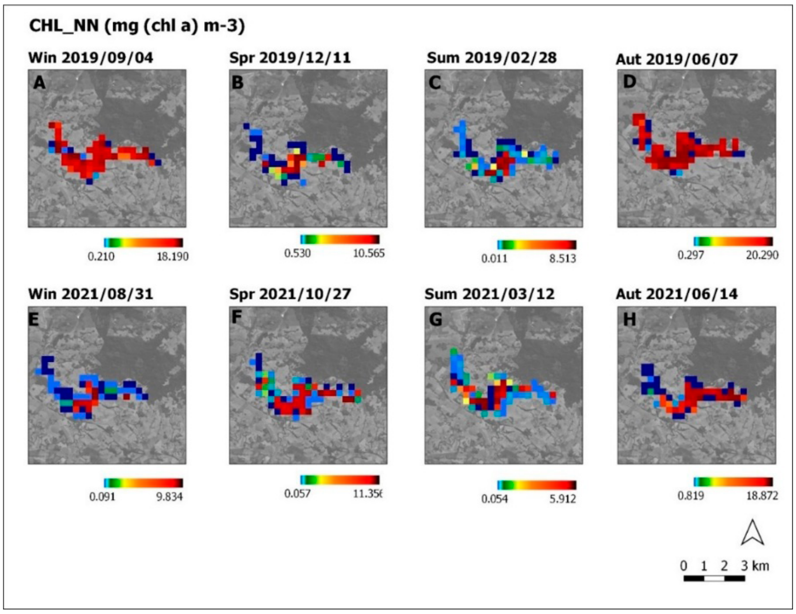

Figure 8: Composite Sentinel-3B OLCI images for chlorophyll-a concentrations (CHL_NN). (A) Winter 2019; (B) Spring 2019; (C) Summer 2019; (D) Autumn 2019; (E) Winter 2021; (F) Spring 2021; (G) Summer 2021; (H) Autumn 2021.

Figure 9 consists of composite Sentinel-3B OLCI images for TMS_NN. In the analyzed period of 2019 (Figure 9(D)), the autumn season showed the highest concentration of water turbidity with a value of 100 (gm-3). Water turbidity for the year 2021 increased in all seasons, indicating a high occurrence of environmental degradation of the water at the Capinguí Dam.

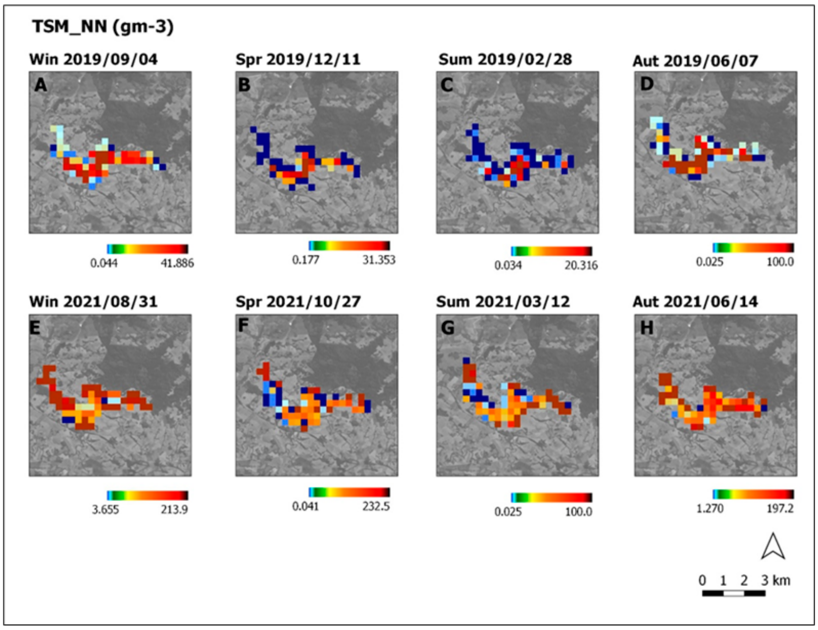

Figure 9: Composite Sentinel-3B OLCI images for Water Turbidity (TMS_NN). (A) Winter 2019; (B) Spring 2019; (C) Summer 2019; (D) Autumn 2019; (E) Winter 2021; (F) Spring 2021; (G) Summer 2021; (H) Autumn 2021.

Through the analysis of data extracted from Sentinel-3B OLCI satellite images, the K-means analysis fits K = 5 (5 Clusters) groupings for a dataset consisting of a total of 37 collection points, where the R^2 value was 0.564, demonstrating that the model provides a good response to the research question. In this relationship, the silhouette index for k=5 clusters was 0.23, demonstrating a low tendency for clustering, showing that the water has great variability in quality throughout the reservoir (Xu et al., 2023).

Clusters 1, 2, and 5 were influenced by the similarities found in water turbidity (TSM_NN) and dissolved material on the surface (ADG443_NN). Cluster 1 was influenced by the summer and spring seasons (Toming et al., 2017). The indices of suspended material and water turbidity may be higher, especially at the water's edge with higher urbanization rates. Cluster 2 was influenced by the winter season, rainfall periods, and rising river water levels. It is normal for there to be a higher concentration of water turbidity (TSM_NN) and dissolved solids (ADG443_NN) at the Capinguí dam (Zhang et al. 2023). Cluster 3 shows greater diversity among the variables; what differentiates this cluster from the others is the role that Chlorophyll-a plays, in all seasons of the year (Li et al., 2024).

Figure 10 shows the results of the clustering using georeferenced data from the 37 points at the Capinguí dam. Clusters 1 and 3 are more related to areas where occupation is more intense, while Clusters 2 and 5 are more related to zones further from the edge.

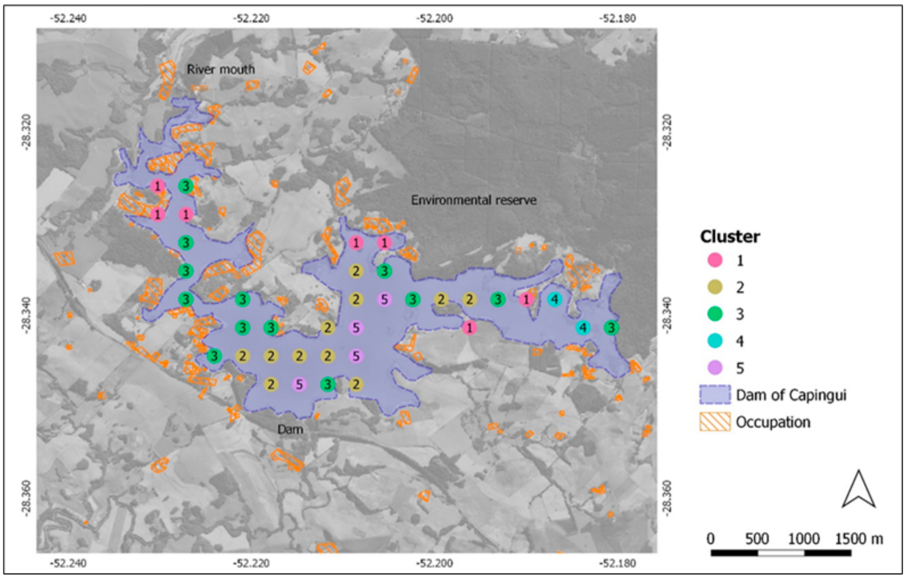

Figure 10: Spatial distribution of clusters in relation to the study area at the Capinguí Dam.

4 Conclusion

Changes in land use have led to increased production, meeting the goals of the UN Sustainable Development Goals (SDGs), especially those related to food security, with a current increase in vegetation area from 1975 to 2020. This study demonstrates that the Landsat 2, 5, 7, and 8 satellites have become efficient for land use analysis (Pahlevan et al., 2022; Hieronymi et al., 2023).

Analyses performed by the Sentinel-3B OLCI satellite, from 2019 to 2021, focused on evaluating water resources, showed high concentrations of suspended material on the water surface (3,830 m-1), chlorophyll-a (20,290 (mg (CHL_NN) m-3)), and water turbidity (100 (gm-3)). It is suggested that this study of the water quality of the Capinguí Dam be continued, in order to identify the real sources of pollution for the development of more public policies that guarantee the preservation of this water resource (Viana et al., 2022; Parven et al., 2022).

The methodology used in this study, which identified the effectiveness of Brazilian public policies in increasing the agricultural production system, linked to environmental preservation, can be used on a global scale, in order to evaluate the levels of local sustainability on a temporal scale through geospatial analyses in other countries of the world, considering the degree of land use on the effectiveness of public policies for environmental preservation (Wulder et al., 2022; Zhu et al., 2023).

Acknowledgments

The authors are grateful to the European Space Agency (ESA) and the U.S. National Aeronautics and Space Administration (NASA) for providing the unpublished and processed images, originating from the Sentinel-3B OLCI satellite. We also wish to thank the Center for Studies and Research on Urban Mobility More Sustainability (NEPMOUR+S), National Council for Scientific and Technological Development (CNPq), Brazil.

Conflicts of Interest: The authors declare no conflict of interest.

Referências

ACUTI, D.; BELLUCCI, M.; MANETTI, G. Company disclosures concerning the resilience of cities from the Sustainable Development Goals (SDGs) perspective. *Cities*, v. 99, p.

ALVARES, C. A.; STAPE, J. L.; SENTELHAS, P. C.; GONÇALVES, J. L. M.; SPAROVEK, G. Köppen's climate classification map for Brazil. *Meteorologische Zeitschrift*, Stuttgart, v. 22, n. 6, p. 711–728, 2013. DOI: https://doi.org/10.1127/0941-2948/2013/0507.

ARBELAITZ, O.; GURRUTXAGA, I.; MUGUERZA, J.; PÉREZ, J. M.; PERONA, I. An extensive comparative study of cluster validity indices. *Pattern Recognition*, Oxford, v. 46, n. 1, p. 243–256, 2013. DOI: https://doi.org/10.1016/j.patcog.2012.07.021.

CEEE – COMPANHIA ESTADUAL DE ENERGIA ELÉTRICA. Usina Hidrelétrica Capinguí. Porto Alegre: CEEE, 2020.

CHOWDHURY, S.; KHAN, S.; SARKER, M. F. H.; ISLAM, M. K.; TAMAL, M. A.; KHAN, N. A. Does agricultural ecology cause environmental degradation? Empirical evidence from Bangladesh. *Heliyon*, v. 8, e09750, 2022. DOI: https://doi.org/10.1016/j.heliyon.2022.e09750.

CUSHMAN, S. A. Calculating the configurational connectivity of landscapes. *Landscape Ecology*, v. 31, n. 2, p. 303–324, 2016.

DONLON, C. J. et al. The Global Monitoring for Environment and Security (GMES) Sentinel-3 mission. *Remote Sensing of Environment*, Amsterdam, v. 120, p. 37–57, 2012. DOI: https://doi.org/10.1016/j.rse.2011.07.024.

ESA – EUROPEAN SPACE AGENCY. Sentinel-3 OLCI User Guide. Paris: European Space Agency, 2021.

FAO – FOOD AND AGRICULTURE ORGANIZATION OF THE UNITED NATIONS. *The future of food and agriculture: Trends and challenges*. Rome: FAO, 2017.

GOODCHILD, M. F.; FU, P.; RICH, P. Sharing Geographic Information: An Assessment of the Geospatial One-Stop. *Annals of the Association of American Geographers*, v. 97, n. 2, p. 250–266, 2007. DOI: https://doi.org/10.1111/j.1467-8306.2007.00534.x.

MCGARIGAL, K.; CUSHMAN, S. A.; ENE, E. *FRAGSTATS v4: Spatial Pattern Analysis Program for Categorical and Continuous Maps*. Amherst: University of Massachusetts, 2012.

PARVEN, A.; PAL, I.; WITAYANGKURN, A.; PRAMANIK, M.; NAGAI, M.; MIYAZAKI, H.; WUTHISAKKAROON, C. Impacts of disaster and land-use change on food security and adaptation: evidence from the delta community in Bangladesh. *International Journal of Disaster Risk Reduction*, Amsterdam, v. 78, p. 103119, 2022. DOI: https://doi.org/10.1016/j.ijdrr.2022.103119.

ROCKSTRÖM, J. et al. A safe operating space for humanity. *Nature*, London, v. 461, n. 7263, p. 472–475, 2009. DOI: https://doi.org/10.1038/461472a.

ROY, D. P. et al. Landsat-8: Science and product vision for terrestrial global change research. *Remote Sensing of Environment*, Amsterdam, v. 145, p. 154–172, 2014. DOI: https://doi.org/10.1016/j.rse.2014.02.001.

SCHOBER, P.; BOER, C.; SCHWARTE, L. A. Correlation coefficients: appropriate use and interpretation. *Anesthesia & Analgesia*, Philadelphia, v. 126, n. 5, p. 1763–1768, 2018. DOI: https://doi.org/10.1213/ANE.0000000000002864.

TOMING, K. et al. First experiences in mapping lakewater quality parameters with Sentinel-3 OLCI imagery. *Remote Sensing*, Basel, v. 9, n. 6, art. 640, 2017. DOI: 10.3390/rs9060640.

TURNER, M. G.; GARDNER, R. H.; O'NEILL, R. V. *Landscape Ecology in Theory and Practice: Pattern and Process*. New York: Springer, 2001.

VIANA, C. M.; FREIRE, D.; ABRANTES, P.; ROCHA, J.; PEREIRA, P. Agricultural land systems importance for supporting food security and sustainable development goals: a systematic review. *Science of the Total Environment*, v. 806, p. 150718, 2022. DOI: https://doi.org/10.1016/j.scitotenv.2021.150718.

WULDER, M. A. et al. Current status of Landsat program, science, and applications. *Remote*

Sensing of Environment, Amsterdam, v. 225, p. 127–147, 2019. DOI: https://doi.org/10.1016/j.rse.2019.02.015.

YIRAN, G. A. B.; ABLO, A. D.; ASEM, F. E. Urbanisation and domestic energy trends: analysis of household energy consumption patterns in relation to land-use change in peri-urban Accra, Ghana. *Land Use Policy*, v. 99, p. 105047, 2020. DOI: https://doi.org/10.1016/j.landusepol.2020.105047.

XU, D.; TIAN, Y. A comprehensive survey of clustering algorithms. *Annals of Data Science*, Singapore, v. 2, n. 2, p. 165–193, 2015. DOI: https://doi.org/10.1007/s40745-015-0040-1.